5-2016

Cell Contraction, De-adhesion, and Shape Effects Investigated by Cohesive Model with Finite Element Simulations

Margarita Vladimirovna Semenova Petrova
University of Tennessee - Knoxville, mpetrov1@vols.utk.edu

To the Graduate Council:

I am submitting herewith a thesis written by Margarita Vladimirovna Semenova Petrova entitled "Cell Contraction, De-adhesion, and Shape Effects Investigated by Cohesive Model with Finite Element Simulations." I have examined the final electronic copy of this thesis for form and content and recommend that it be accepted in partial fulfillment of the requirements for the degree of Master of Science, with a major in Materials Science and Engineering.

Yanfei Gao, Major Professor

We have read this thesis and recommend its acceptance:

Wei He, Xiaopeng Zhao, Claudia Rawn

Accepted for the Council:
Carolyn R. Hodges

Vice Provost and Dean of the Graduate School

(Original signatures are on file with official student records.)

Cell Contraction, De-adhesion, and Shape Effects Investigated by Cohesive Model with Finite Element Simulations

A Thesis Presented for the

Master of Science

Degree

The University of Tennessee, Knoxville

Margarita Vladimirovna Semenova Petrova

May 2016

Acknowledgements

I would like to express my greatest appreciation to my advisor, Professor Yanfei Gao for his time and the great effort to guide my research. His guidance provided me with an excellent opportunity to be involved in this exciting research, to explore, and challenge my research potential. Professor Gao's enthusiasm and outstanding knowledge supported me all the way during my research.

Also, I would like to express the gratitude to my co-advisor, Dr. Wei He, for her time and support, and to other committee members, including Dr. Xiaopeng Zhao and Dr. Claudia Rawn. I would like to thank my research group members and all people who offered valuable discussions, advice, and assistance on different topics associated with my research including finite element simulations. I enjoyed working with my friends and colleagues, including Chao Pu, Peijun Hou, Wei Zhang, Professor Zhiwen Gao and many others.

Abstract

Cell adhesion is a complex mechanism, and different factors control this process including surface morphology, chemical, and mechanical interactions. These aspects are usually combined to achieve robust adhesion between surfaces. The later stage in bio-adhesion process involves the formation of molecular bonds through diffusion or interpenetration of molecules at the interface. In order to create contact, cells sense their physical environment by applying mechanical forces or responding to them via traction force. The force is transmitted through cell skeleton. However, how this force is transmitted is mostly unknown. Also, there are still many open questions about fracture mechanism in bio-adhesive contacts. What is the critical shear stress that separates cell from substrate? Which role plays cell contraction in the process of de-adhesion? What is the influence of the cell shape effect, the effect of contractile cell strain and fracture energy on the critical stress at separation?

These open questions are addressed by studying cell contraction, de-adhesion, and shape effects investigated by cohesive model with finite element simulations. Cell-substrate system is modeled as a pre-strained elastic disk which is attached to elastic substrate via molecular bonds at the bio-adhesive interface. The effect of fracture energy on the critical stress at separation with constant contractile cell strain; and the effect of contractile cell strain on the critical stress at separation with constant fracture energy have been investigated in this research. Then both effects on the critical stress at separation have been compared. The effect of cell shape on the critical stress at separation has also been studied in this research. It is confirmed that de-adhesion is controlled by the transition from small-scale bridging (SSB) behavior to large-scale bridging (LSB) behavior by the dimensionless parameter, the ratio of the crack-bridging zone size to the contact radius, which has important consequences for the design of biomimetic and the achievement of optimized adhesion force.

Table of Contents

List of Tables

List of Figures

Chapter 1

Introduction and General Information

1.1 Bioadhesion phenomena

Bioadhesion represents the phenomena in which different materials (natural and synthetic) adhere to biological surfaces. Bioadhesion refers to the use of bioadhesives to bond surfaces together which is relevant for many biomedical applications, including dental and surgery. Bioadhesion represents a great interest for research due to its implications to design of new materials and technological products.

Bioadhesion is similar to conventional adhesion in many ways. Macroscopic surfaces will not have strong adhesive forces due to the surface roughness, and the net adhesion force is relatively small [24]. During evolution biological systems have been developed hierarchical structures to maximize adhesion force. A good example of adhesion through hierarchical structures is demonstrated by the movement of gecko on various surfaces including vertical walls and ceilings. In bioadhesive contacts a good attachment to rough surfaces and readily releasable detachment from them is important for gecko to move successfully on vertical surfaces [1]. Good adhesion helps the animal “stick” to a rough surface when it moves along it. Another example of bioadhesive contacts is focal contacts which contain the clustering of molecular receptor-ligand bonds which play an important role in bioadhesion.

1.2. Factors in bioadhesion

Bioadhesion is a complex mechanism, and different factors control it. They include surface morphology, chemical, and mechanical interactions. These aspects are usually combined

to achieve a good adhesion between surfaces. If two surfaces form covalent, ionic, or metallic bonds, strong adhesion is achieved between these surfaces. At the same time, weaker forces such as hydrogen bonding or Van der Waals interactions also make contribution in bonding between surfaces [2]. Chemical bonding and the interface between surfaces play the leading role in the earlier stages of bioadhesion. The later stage involves the formation of molecular bonds between contacting surfaces achieved through diffusion of molecules at the interface.

1.3. Traction force

Cells probe their physical environment by pushing, pulling, and imposing traction forces on surrounding surfaces. The forces are transmitted through cell skeleton. Studies show that traction forces play a big role in the process of cell migration [1]. The considerable attention has been given to study the distribution of traction forces lately including the mechanism which controls the distribution of traction forces and the distance from cell center.

1.4. Non-uniform breaking of molecular bonds and releasable bioadhesion

Many biological contacts have hierarchical structurers as in the case of gecko with the clusters of small hairs on their feet. When these bonds are broken, the transition from Griffith limit to uniform stress limit is governed by the ratio of the crack bridging zone size to the contact radius [23-24]. An important problem in bioadhesive contacts is an orientation-dependent adhesion strength. In hierarchical structures discrete bonds are realigned in different loading directions to achieve easy releasable adhesion, and pull off force varies with pulling direction. Also, pull off force depends on the evolution of crack morphology influenced by the initial contact area shape [5].

1.5. Cohesive model and finite element simulations

Computational technique with finite element method is used to simulate cell-substrate system as deformable solids using the commercial finite element program ABAQUS 6.12 with the purpose to study cell contraction, de-adhesion, and shape effects in bio-adhesive contacts.

The initiation and propagation of crack at the interface during de-adhesion process is investigated with cohesive model. According to this model, there is cohesive zone ahead of crack tip at the interface, which consists of upper and lower surfaces held by cohesive traction. The cohesive traction at the interface is related to the separation displacement between the upper and lower surfaces. When surfaces are pulled apart, traction forces increase till maximum is reached, then they gradually decrease to zero, at which complete separation takes place. The model mathematically reflects continuity conditions to avoid stress singularity even if physical separation takes place. The dependence of traction to displacement is plotted on the curve called the traction-displacement curve. The area under the curve represents the energy necessary for separation. More important, this model is limited to cohesive strength of the material.

1.6. Motivation and outcome of this research

Models created in this study integrate cell contractility and cell shape effects with fracture via breaking molecular bonds at the interface. The main focus of the paper by He et al. [1] related to this research was to study the distribution of traction forces for cell-substrate system during mechano-sensing. The displacement and stress fields are obtained by modeling cell-substrate system as a pre-strained elastic disk attached on elastic substrate via molecular bonds. However, this model does not consider fracture of the interface. Releasable adhesion involving fracture of the interface has been studied in another relevant paper by Liu and Gao [5].

However, their cohesive model does not consider a pre-strained condition for cell in bioadhesive contact.

The objectives of this research are to study effect of fracture energy on the critical stress at separation with constant contractile cell strain, effect of contractile cell strain on the critical stress at separation with constant fracture energy, and to compare both effects on the critical stress at separation. Also, the additional research objectives include the study of cell shape effect on the critical stress at separation and the confirmation of the role of the crack-bridging characteristics in the transition from small-scale bridging behavior to large-scale bridging behavior. The major outcome of this study is aimed at the improvement of our understanding of cell contraction, de-adhesion, and shape effects in cell-substrate system which can shed light on the design of biomimetics and releasable adhesives.

Chapter 2

Literature Review

2.1. Hierarchical structures and focal contacts in bioadhesion

The area of bioadhesion is of a particular interest for researchers who study fundamental mechanisms that govern bioadhesion. Cell and substrate materials have a rough microscopic surface at the area of contact (Fig. 2.1). The adhesion force is very small due to this roughness. Many biological systems developed hierarchical structures to solve this problem including many insects and gecko which very many small hairs on their feet called spatulae. The advantage of hierarchical structure is that adhesion is improved with each level in the hierarchy, (Fig.2.2). According to the study conducted by Liu and Gao [5], a small diameter of each hair in gecko's feet provides a uniform stress distribution during de-adhesion to avoid crack-like behavior.

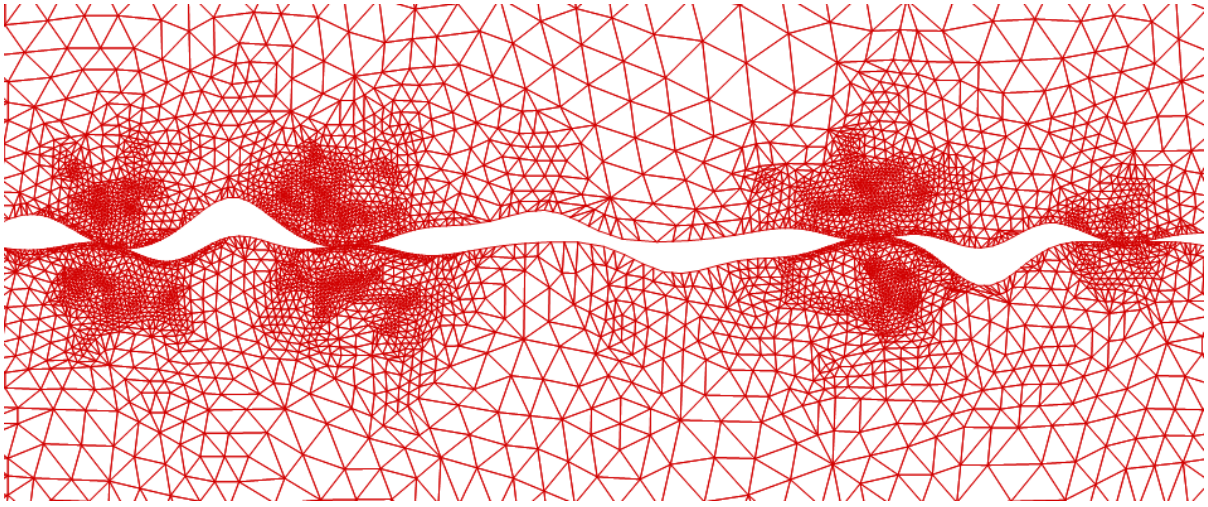

Figure 2.1. Engineering surfaces are rough at the area of contact [25].

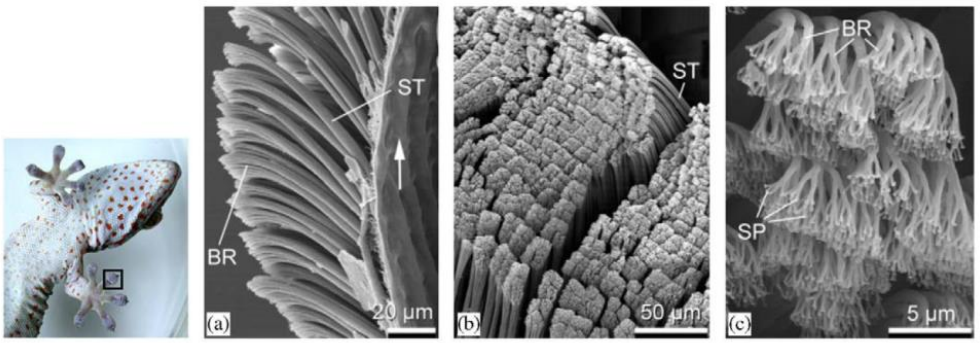

Figure 2.2. Gecko toe's structure has an improved adhesion in each level of the hierarchy [26].

Besides hierarchical structures, cell adhesion can be accomplished through the clustering of receptor-ligand bonds into focal-adhesion contacts through which mechanical force and regulatory signals are transmitted. Adhesion and de-adhesion of focal contacts cause elastic deformation of the surrounding material as cells probe their physical environment by pushing, pulling, and imposing traction forces on surrounding surfaces.

2.2. Transition from Griffith crack to the uniform stress limit

The process of de-adhesion can be represented by interface fracture problem with external crack. The stress near the contact edge is approaching infinity at the limit of Griffith crack, and fracture happens as in the case of brittle materials. As the interface consists of long-chain molecules, the low interface stiffness reduces the stress singularity at the contact edge. In this case, the entire interface has uniform stress as in the example of gecko pulling off its toes with very many small hears [5]. There is a transition from Griffith limit to the uniform stress limit governed by the stress concentration index [6]. More interesting, de-adhesion has a transition from small scale-bridging (SSB) behavior with Griffith crack to large-scale bridging (LSB) behavior with a uniform stress limit. During releasable adhesion discrete bonds realign asymmetrically with different pull off force depending on the loading direction. Crack

morphology influences extremal values of pull off force, and it is inversely proportional to the contact stiffness contours. The maximum and minimum peeling forces are related to the highest and lowest contact stiffness [5].

2.3 Mushroom-shaped fiber

Another interesting phenomenon of cell adhesion in hierarchical structures is a shape of the smallest unit. Many hierarchical structures have a mushroom shape of fiber instead of a cylindrical shape. It is shown by Liu et al. [7], that normal stress field diverges at the contact edge when the fiber with cylinder shape is pulled off the substrate. In contrast, the fiber with a mushroom shape has reduced stiffness at the contact edge. As the result, the degree of normal stress singularity at the interface is reduced, (Fig. 2.3).

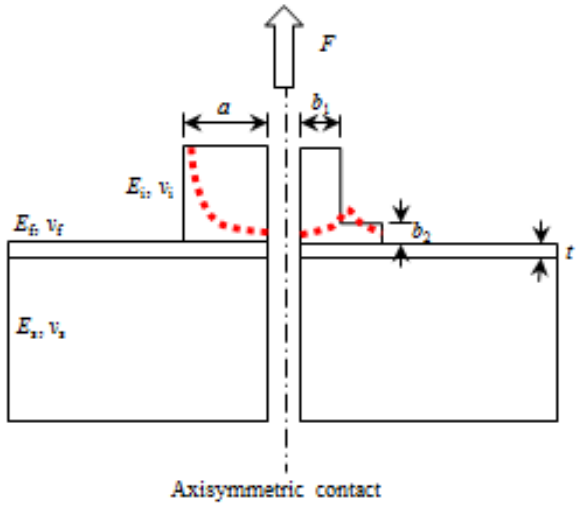

Figure 2.3. Mushroom-shaped fiber in bio-adhesive contact [7].

An important principle in linear elastic fracture mechanics (LEFM) is stress singularity if a part has geometry with sharp corners. The interaction between surfaces in bio-adhesive contacts at small-scale length has finite strength. This interaction follows the traction-separation

law in cohesive zone model [7]. This law says that stress increases at separation of the interface then it reaches maximum value and gradually comes to zero which is not possible in LEFM. LSB behavior dominates in adhesion of hierarchical structures as in the case of gecko when the entire crack surface experiences stress equivalent to interface strength. As a result, the de-adhesion force depends on interface strength and the contact area [8]. It is shown by Liu et al. [7] in the model implemented into the commercial finite element software ABAQUS, that mushroom-shaped fibers can improve the adhesive performance if the interface has SSB behavior (Fig. 2.4). The introduction of additional compliance at the contact edge makes the stress intensity factor smaller. In contrast, the mushroom shape does not provide any benefits in LSB behavior limit as the interface is likely to experience de-adhesion in the center of contact.

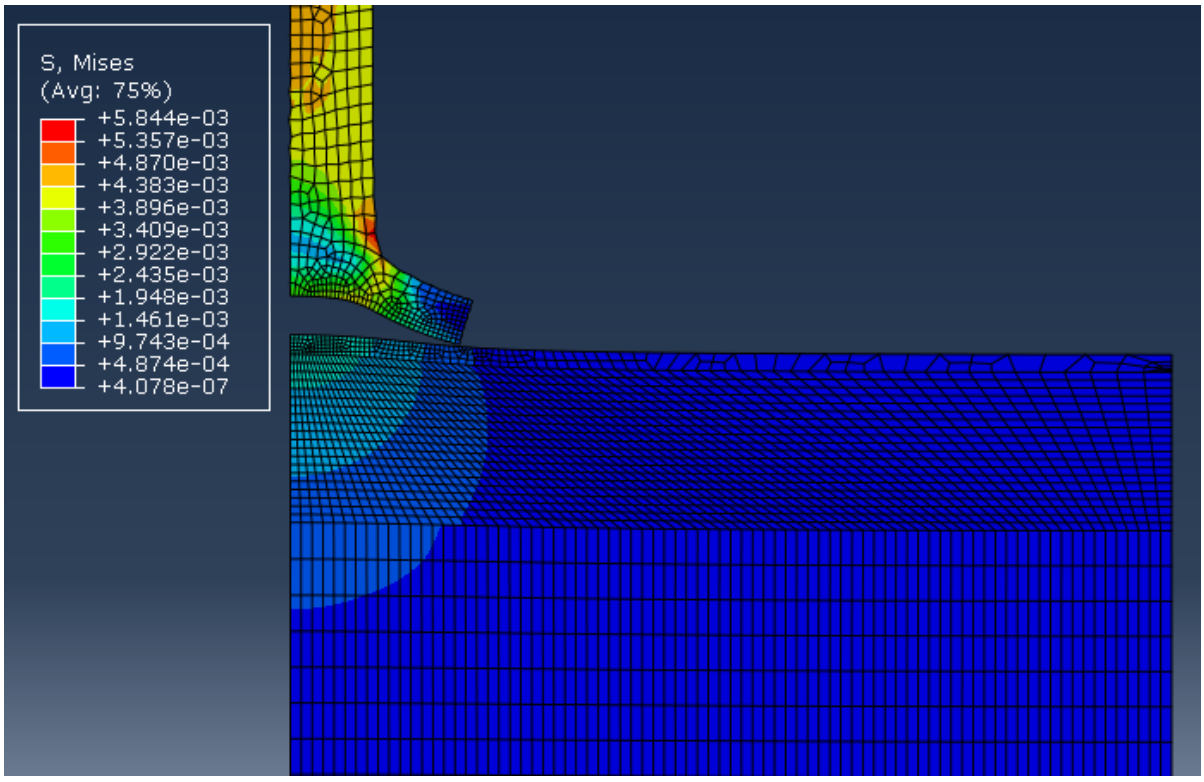

Figure 2.4. The model with mushroom-shaped fiber implemented in ABAQUS [7].

2.4. Traction forces in bioadhesive contacts

Cells probe their physical environment by applying mechanical forces or responding to them during mechano-sensing. It is done by imposing traction forces transmitted through cell skeleton. Studies show that traction forces play a big role in the process of cell migration [1]. Considerable attention has been given to studying the distribution of traction forces lately. The knowledge of the traction force distribution is important for understanding of cell adhesion mechanism. It is observed by Rape et al. [9], that the sizes of focal adhesion complexes (FACs) through which cell skeleton connects to extra-cellular matrix (ECM) and the traction forces are proportional to the distance from cell center, (Fig. 2.5). ECM represents a collection of extra cellular molecules secreted by cells that provides structural and biomedical support to the surrounding cells. It can be seen that the bigger the distance from cell center is, the bigger the magnitude of traction force. Also, the polarized cell shape influences the distribution of traction forces [9]. The dependence of traction force on the distance from cell center was also studied by Gardel et al. [10]. They show that cell traction increases with the distance from cell center. A cell shape and size can be measured based on the magnitude of traction force based on the requirement to satisfy the condition of mechanical equilibrium [9, 11].

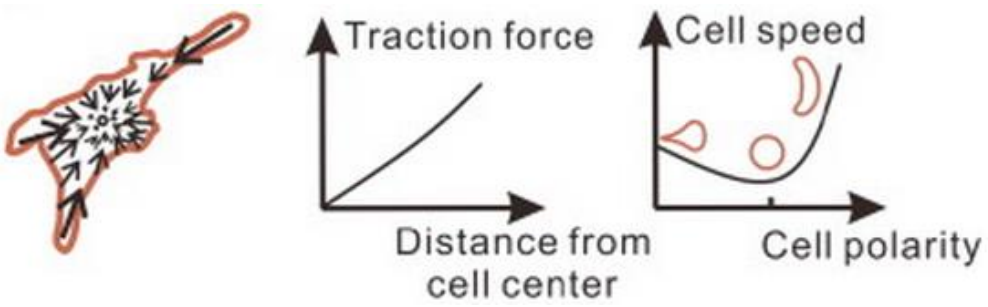

Figure 2.5. Cell traction depends on the distance from cell center. The polarized cell shape influences the distribution of traction forces [9].

Quite a number of theoretical models on cell adhesion and the distribution of traction forces have been developed to see if they support experimental data. For example, JKR model is created by Chen and Gao [12], where stability analysis of cell adhesion is performed when substrate is stretched. Modeling of cell as a set of fibers experiencing stress with uniform pre-strain under tension is created by Lemmon and Romer [13]. They studied the distribution of cell traction forces on cell-substrate system. Model of cell layer on micro-posted substrate is developed by Edwards and Scwartz [14]. They treated micro-posts as elastic springs and obtained the results showing that the traction force distribution is the highest at the edge of the layer. The displacement in substrate decays with the distance from cell edge and with the depth from the contact surface. This decay length is comparable to cell size. In fact, cell size is a quantitative measure of how far cell pushes or pulls into its physical environment. [1]. When cell contracts during mechano-sensing, it induces strain which is larger on thinner gels (about 500 nanometers) then on thicker gels (around 70 micrometers) [15]. Study on the distribution of displacement and strains on gel surfaces conducted by Sen et al. [16] shows that the displacement and strain decline with the distance away from cell periphery, (Fig. 2.6).

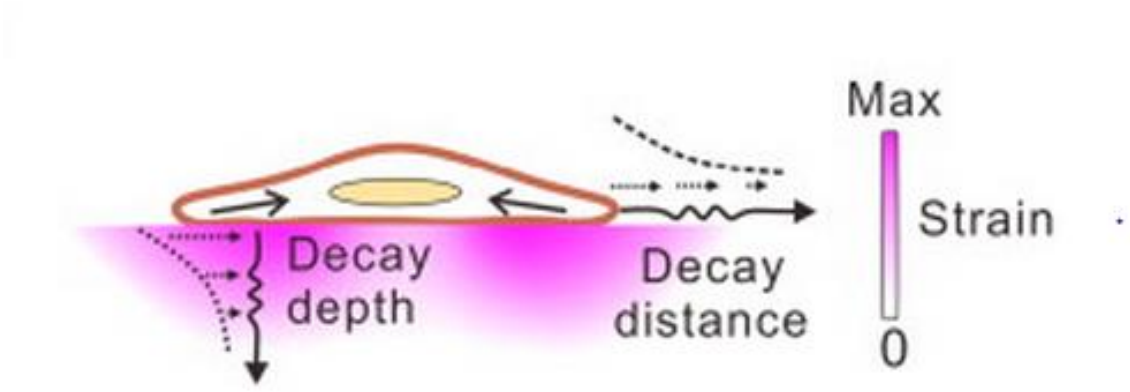

Figure 2.6. Cell induced deformation field in substrate deteriorates with the depth and distance from the peripheral area of cell [16].

A few other models involving cell contraction during mechano-sensing have been developed. For example, cell is modeled as a network of stress fibers with a uniform tensional pre-strain in the study conducted by Lemmon and Romer [13]. Deshpande et al. [17] consider the dynamic reorganization of skeleton and FACs to model cell contraction when cell interacts with substrate. It is shown, that FACs group into the clusters at cell periphery.

2.5. The role of substrate stiffness on the distribution of traction forces

Cells probe the stiffness of substrate based on how much material deforms when stress is applied [18]. Substrate stiffness plays an important role in mechano-sensing of cells due to effect of traction forces at the interface of cell-substrate system. Interesting observation is made by Fu et al. [19] that traction force, cell spreading area, and total area of focal adhesion complexes increase with the stiffness of micro-posts. According to Ladoux et al. [20], average force on micro-posts increases linearly with the post stiffness when the pillar stiffness is soft, but when it reaches a certain value of stiffness, it stays constant [20], (Fig. 2.7). This phenomenon shows that cell adhesion behavior can be controlled by substrate stiffness.

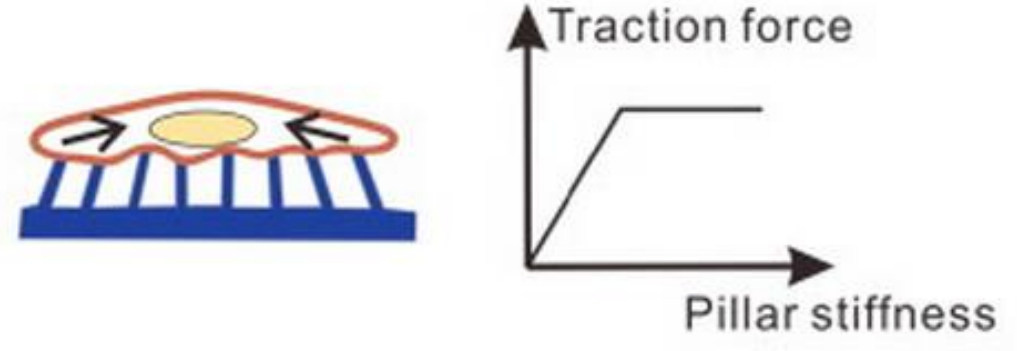

Figure 2.7. Cell imposes traction forces on micro-posts of the substrate. Cell traction depends on the stiffness of micro-posts [20].

2.6. Open questions in bioadhesive contacts

Considerable attention in recent studies of bio-adhesive contacts has been given to mechanism of de-adhesion and what governs this process; the effect of mushroom-shaped fiber on the distribution of traction forces at the interface of cell-substrate system; and the role of substrate stiffness in cell adhesion behavior. However, there are still many open questions. How does cell shape influence the distribution of traction forces in de-adhesion process? What is the effect of contractile cell strain and fracture energy on the critical shear stress that separates cell from substrate? What is the cell shape effect on the critical stress at separation and the transition from SSB behavior to LSB behavior? Cell contraction, de-adhesion, and shape effects have been investigated by cohesive model with finite element simulations to study and clarify these questions.

Chapter 3

Cohesive Interface Simulations

The commercial finite element program ABAQUS is used to study cell contraction, de-adhesion, and shape effects in bioadhesive contacts. Cell is modeled as a pre-strained elastic disc due to the contractility of cell skeleton [17]. When cell adheres on an elastic substrate, it produces deformation in the substrate and traction force. Experimental studies show that the magnitude of cell pre-strain (ε) is about 0.1 according to the physiological conditions [21]. Cell contraction is modeled in ABAQUS by the mismatch of thermal expansion coefficients in cell-substrate system and the reduction of temperature in step one. Then shear load is applied on the cell top surface in step two, and stress fields are calculated for both steps.

At the beginning of the study 2D perfect bonding model is developed. There is no crack propagating at the interface under the stress as molecular bonds between cell and substrate are perfect in this model. The stress concentration field is calculated at the contact edge for both steps (Fig.3.1) to see if the model works correctly. After achieving this task, the study of crack propagation at the interface is extended to 2D cohesive zone model and 3D cohesive zone model with circular and irregular cell shapes.

3.1. Finite element analysis

Finite element analysis is used as technique to study cell-substrate system as deformable solids. This numerical technique solves boundary value problems through a set of partial differential equations.

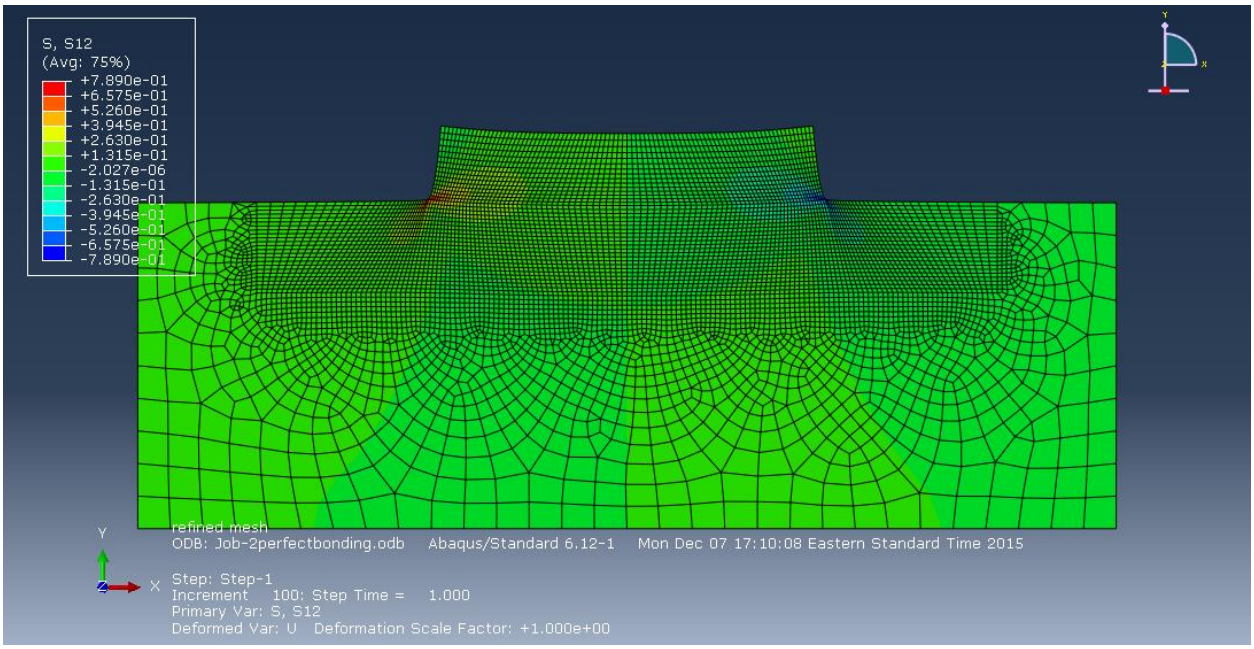

(a)

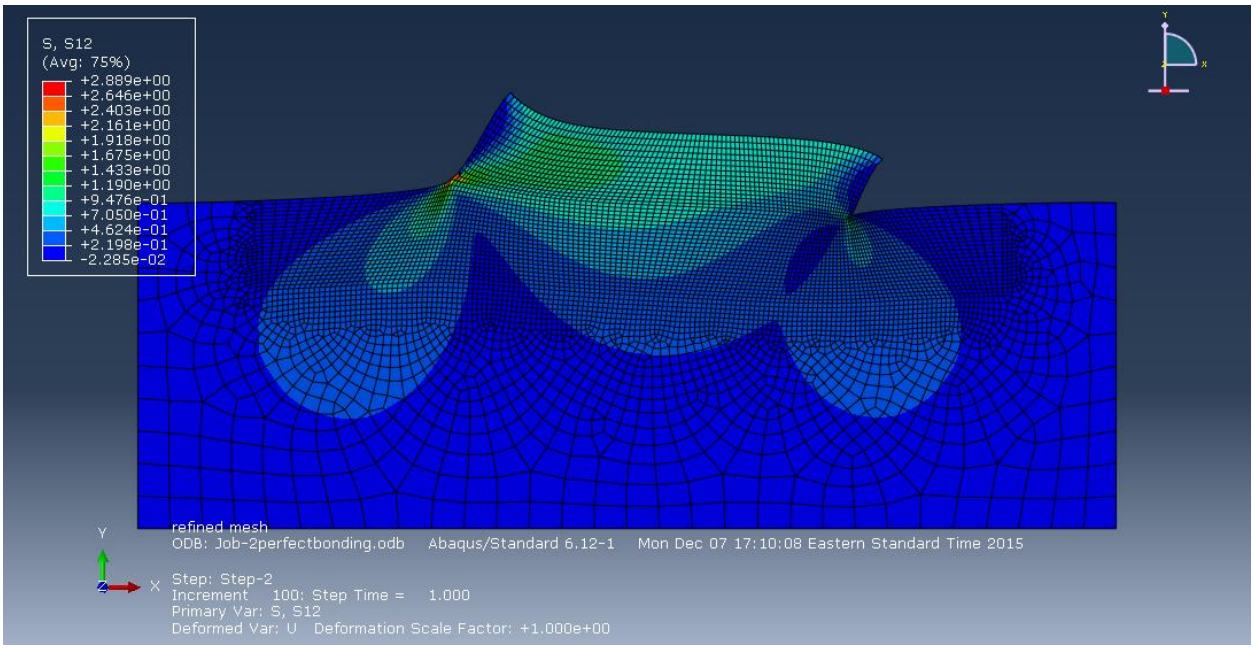

(b)

Figure 3.1. (a) 2D perfect bonding model with stress concentration field at the contact edge, at step one; (b) 2D perfect bonding model, shear load is applied on the cell top surface, at step two.

The first step involved in this method is the division of domain into a set of subdomains (finite elements) where each subdomain represents element equations. It is similar to the idea when circle can be approximated through many tiny lines. In the first step element equations approximate original equations which are more complex partial differential equations in many cases. In the second step, the program generates global equations from element equations via the transformation of coordinates of local nodes within subdomains to the coordinates of global nodes from the main domain. Software with finite element method uses coordinate data generated from subdomains to perform this transformation. After calculations are performed, the data of interest is extracted from the numerical solution obtained through the post-processing procedures.

3.2. Finite element procedure

The geometry of the solid, boundary conditions, history of loading, and material behavior are inputted into the program at the beginning of the study. Then the program calculates the deformation of the solid under applied conditions, stress distribution, and other physical quantities of interest.

3.2.1. Materials

Cell-substrate system is modeled as a pre-strained elastic body which adheres on elastic substrate with the material properties which are elastic isotropic. They are listed in Table 3.1.

Table 3.1. Material properties for cell-substrate system.

Part	Young's Modulus, kPa	Poisson's Ratio	Expansion Coefficient
Cell	10	0.3	0, 0.05, 0.01
Substrate	10	0.3	0

3.2.2. Mesh

The mesh module uses a variety of techniques to generate mesh. The solid is discretized into the number of nodes which are discrete points inside this solid. Each node has its own number for its identification. Any order could be used to number them and then each node is assigned a set of coordinates. For example, for 2D models the set of coordinates is (x_1, x_2) and for 3D models the set of coordinates is (x_1, x_2, x_3). These coordinates determine the position of the solid before it is deformed. When the solid is deformed, each node changes its positon. In 2D models there are two displacement components $(u_1, u_2,)$ for each node. In contrast, there are three displacement components $(u_1, u_{2,}u_3)$ in 3D models. These displacements represent unknown variables at the beginning of analysis, which are calculated by the program.

The mesh module is used to specify the geometry of cell-substrate system and describe the displacement field as a result of deformation. Cell and substrate parts are divided into the number of elements (spatial discretization). The mesh is designed in such way that mesh density becomes high at high stress areas (Fig. 3.2). The hexahedron elements are used in the mesh module for all models in this study. Also, linear elastic behavior and infinitesimal deformation are chosen because they are user friendly in regard to calculation time.

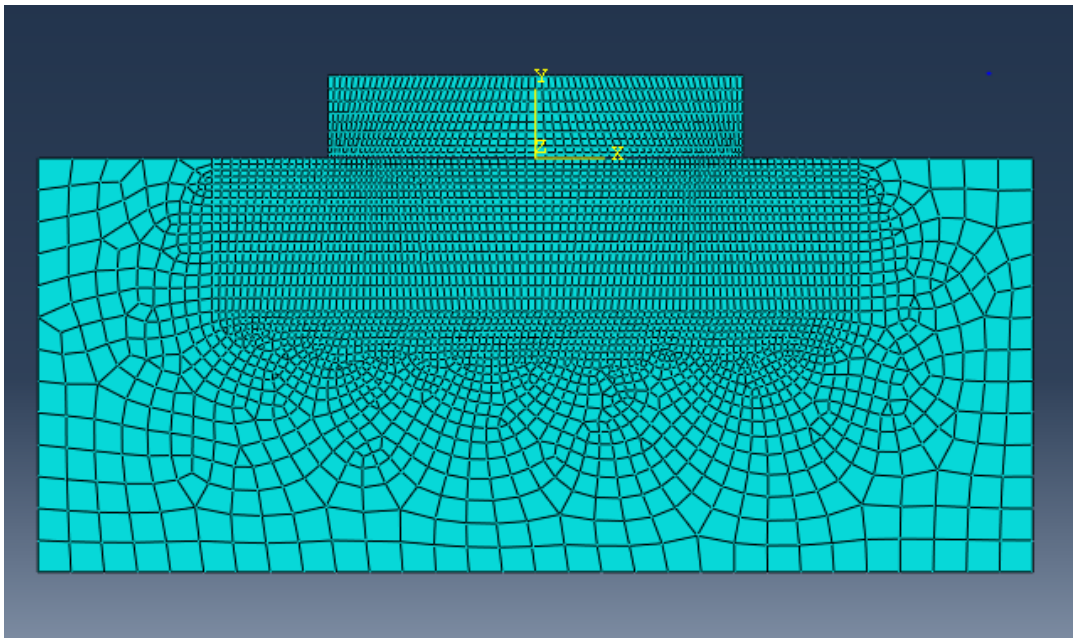

(a)

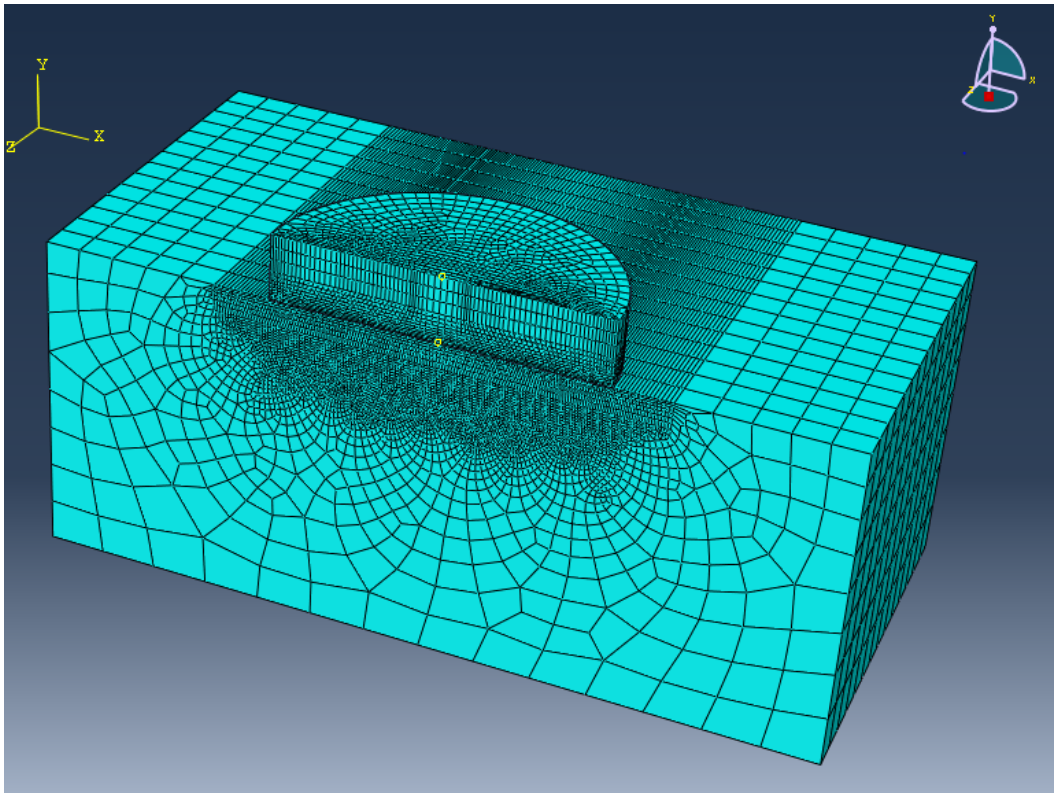

(b)

Figure 3.2. (a) Mesh for 2D cohesive zone model; (b) Mesh for 3D cohesive zone model with circular shape.

3.2.3 Boundary conditions

Boundary conditions for 2D perfect bonding model and 2D cohesive zone model are used so that substrate is fixed from all sides, and its motion including rotation is not allowed along x and y axes. Due to symmetry in 3D model, only one half of the model is created to reduce computational time. It leads to the enforcement of additional symmetry boundary condition to fix the plane where the cut is made, so that this cut plane cannot move or rotate (Fig. 3.3 - 3.4).

3.2.4. Step module

There are two steps applied to the system in step module. In the first step, stress field is created as a result of cell contraction due to the mismatch in thermal expansion coefficients for cell-substrate system and the reduction in temperature. In the second step, temperature is held constant, and shear load is applied at the cell top surface, (Fig. 3.5).

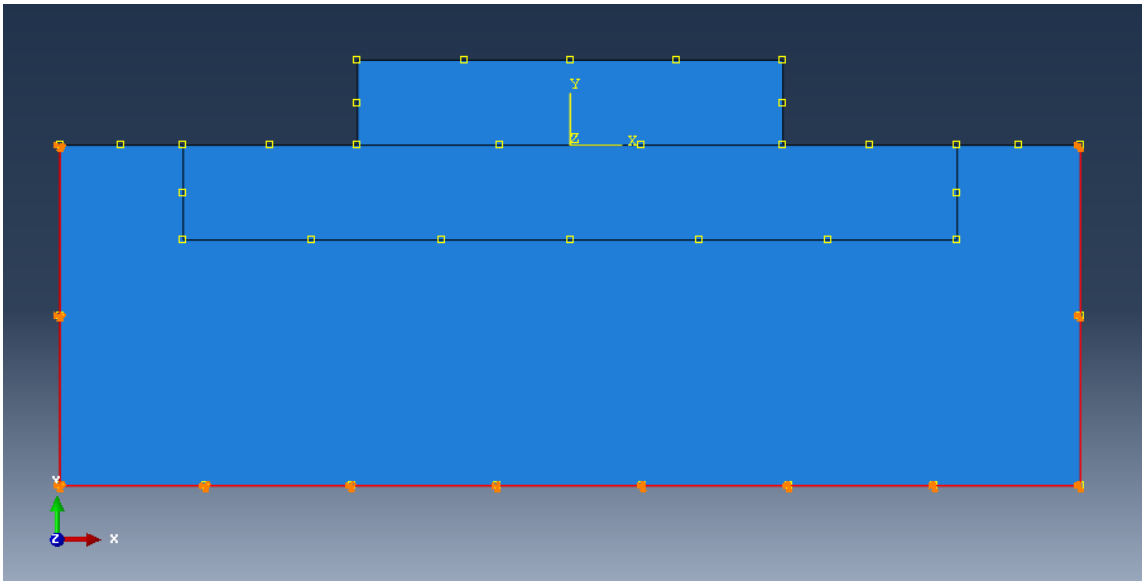

Figure 3.3. Boundary conditions in 2D cohesive zone model: displacement and rotation are constrained along x and y axes.

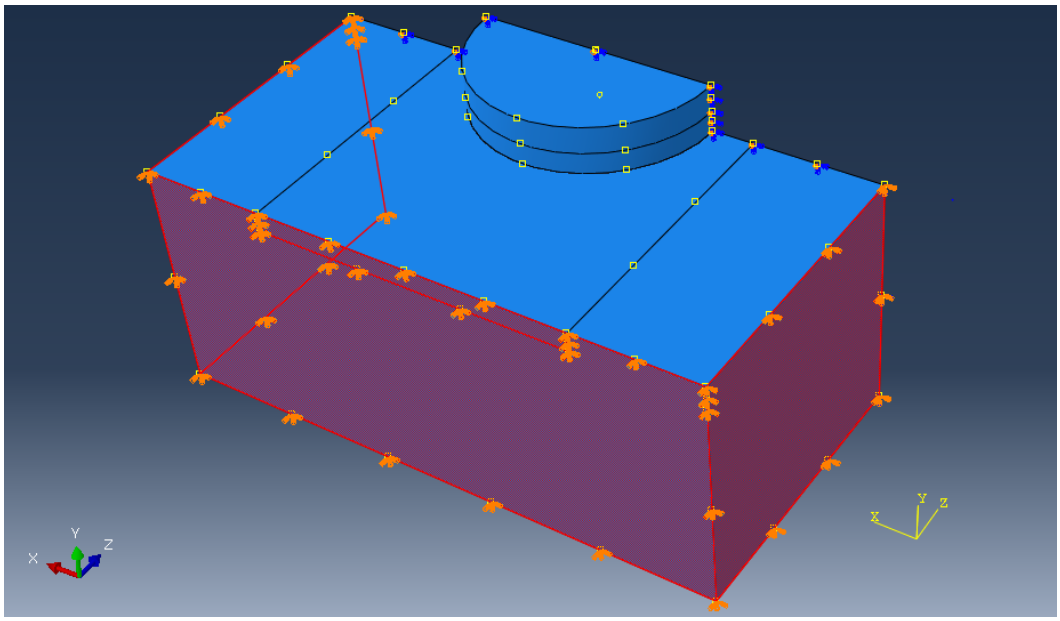

(a)

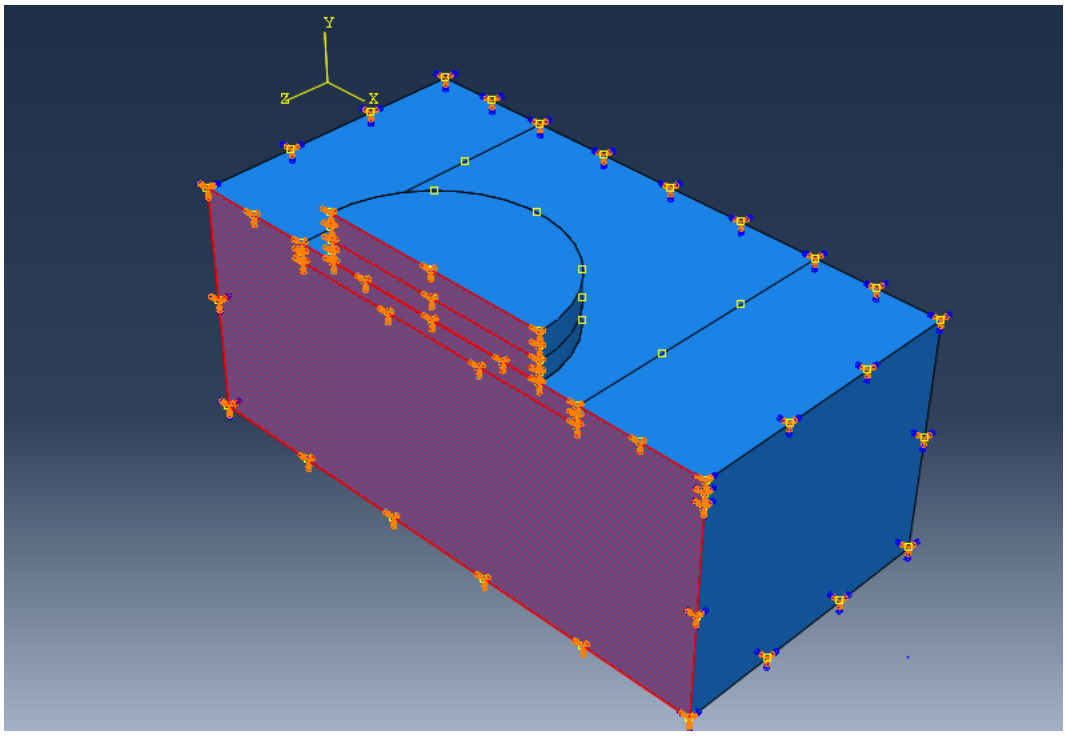

(b)

Figure 3.4. (a) The first boundary condition in 3D cohesive zone model with circular shape: displacement and rotation are constrained along x, y, and z axes; (b) The second boundary condition in the same model: Symmetry/Antisymmetry/Encastre type is chosen due to symmetry when displacement and rotation are constrained along z axis: U3=UR3=UR2=0.

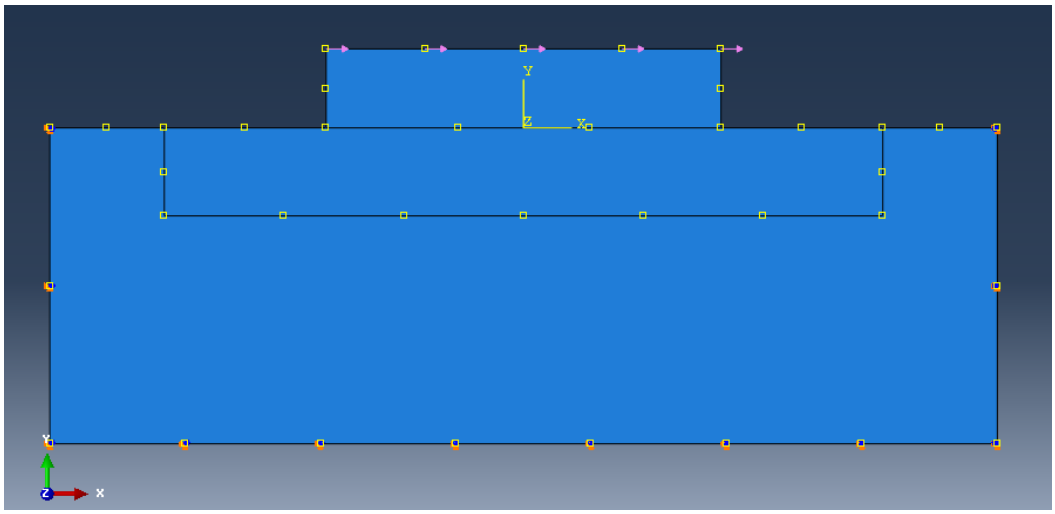

(a)

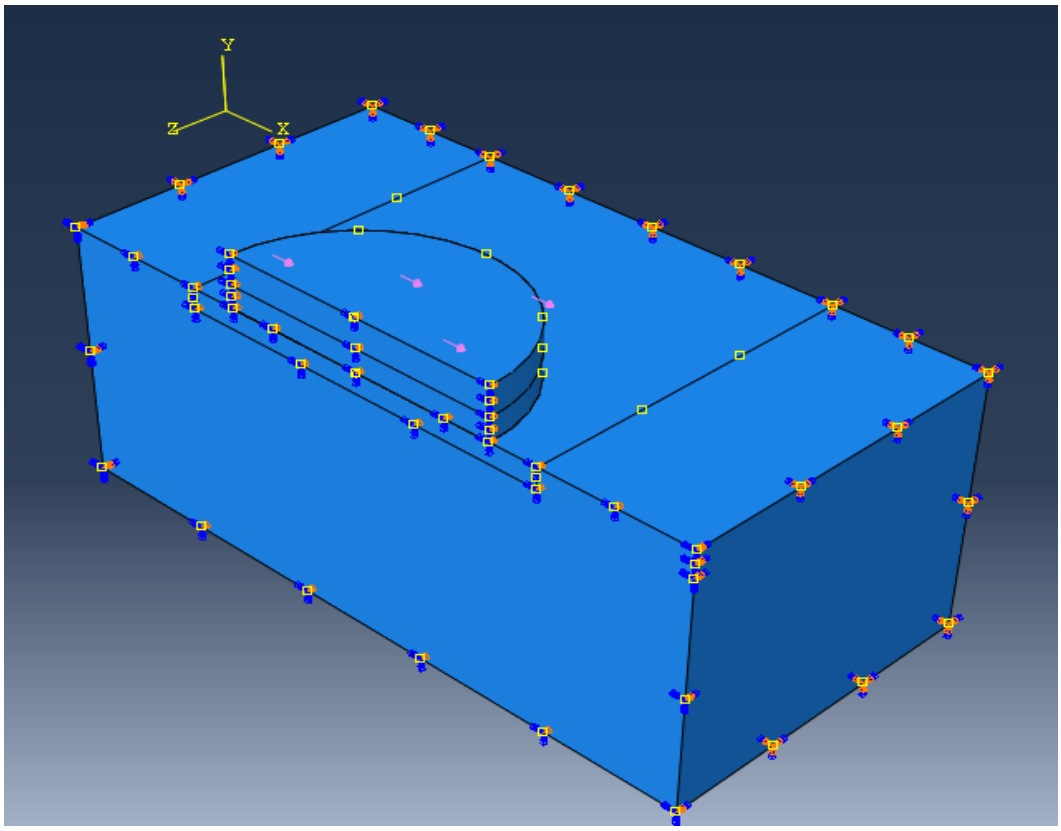

(b)

Figure 3.5. (a) Shear load with surface traction type and uniform distribution is applied on the cell top surface in 2D cohesive zone model; (b) Shear load with surface traction type and uniform distribution is applied on the cell top surface in 3D cohesive zone model with circular shape.

3.3. Cohesive zone model

The cohesive zone model (CZM) is used to analyze behavior of the interface for cell-substrate system. The model simulates the separation of surfaces in contact resisted by cohesive traction forces. The extended crack tip is called cohesive zone. When surfaces are pulled apart, traction forces increase till maximum is reached, then they gradually decrease to zero at which the complete separation takes place. The dependence of traction to displacement is plotted on the curve called the traction-displacement curve, (Fig. 3.6). The area under the curve represents the energy necessary for separation. The model mathematically reflects continuity conditions to avoid singularity of stress even if physical separation takes place. This model is limited to the cohesive strength of material. The principal of virtual work is given by the equation:

$$\int_V \sigma_{ij}\ \delta u_{ij}\, dV + \int_{\Gamma_{int}} T_i \delta \Delta_i\ dA = \int_{\Gamma_s} t_i \delta u_i\, dA$$

The cohesive zone model defines the relationship between traction T_i and separation Δ_i .
The normal and tangential displacement discontinuity across the cohesive interface, (Fig. 3.7) is defined by the equation:

$$\Delta_n = (u^+ - u^-)\, n,\ \Delta_{ta} = (u^+ - u^-)\, t^a,$$

where tractions are: $T_n = n\, \sigma\, n, \quad T_{ta} = n\, \sigma\, t^a$.

In summary, cell contraction, de-adhesion, and shape effects have been investigated by cohesive model with finite element simulations. The finite element commercial software ABAQUS version 6.12 has been used to achieve the computational purposes of this study.

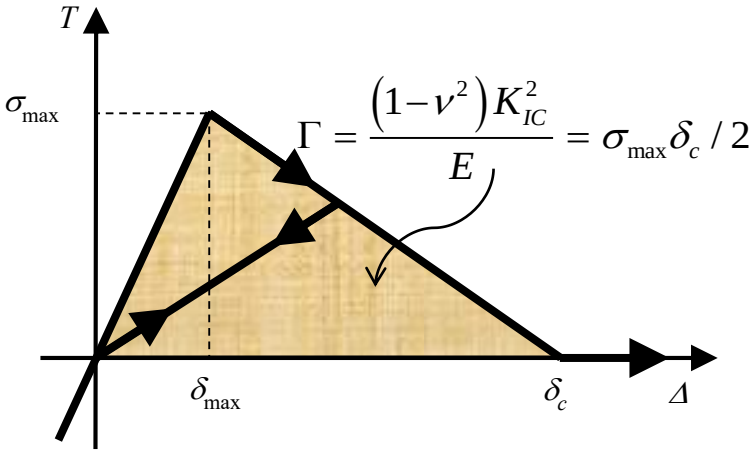

Figure 3.6. Cohesive zone model [27].

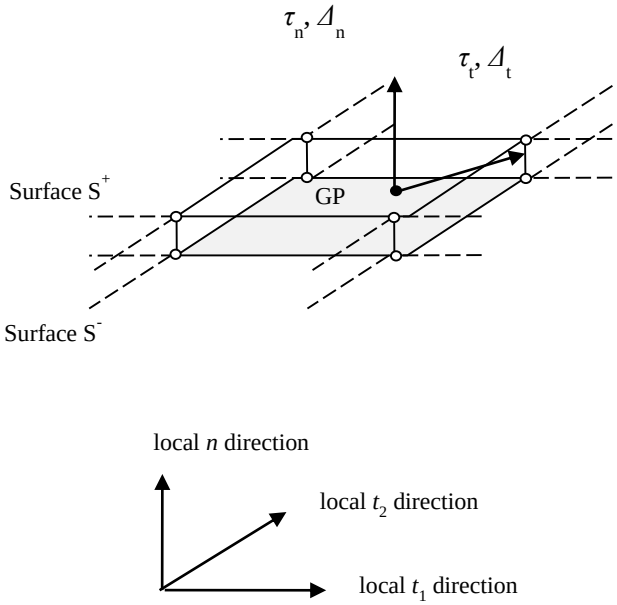

Figure 3.7. Finite element simulations require the projection of traction and separation on the S^+/S^- plane. GP denotes Gaussian integration point in the finite element method [27].

Chapter 4

Results and Discussion

4.1. 2D perfect bonding model

At the beginning of this study, 2D perfect bonding model (PBM) of cell-substrate system is created with the commercial finite element software, ABAQUS/CAE version 6.12. Stress concentration field at the contact edge of the interface is calculated (Fig.4.1). It can be observed that shear stress σ_{12} in step two after shear load is applied on the cell top surface is higher than shear stress σ_{12} in step one when cell contracts due to the mismatch in thermal expansion coefficients and the reduction in temperature.

4.2. 2D cohesive zone model

After the creation of 2D PBM, the study is extended to 2D cohesive zone model (CZM). The comparison of shear stress σ_{12} at step one for both models is shown in Fig. 4.2. This figure plots calculated shear stress σ_{12} at the interface at step one as function of true distance along the path for 2D PBM and 2D CZM. If true distance along the path is in smaller range, shear stress in 2D PBM is larger than in 2D CZM. Shear stresses for both models overlap in the range of true distance path 15 – 39 μm. The magnitude of shear stress for values of true distance path over 39 μm is greater for 2D PBM than for 2D CZM.

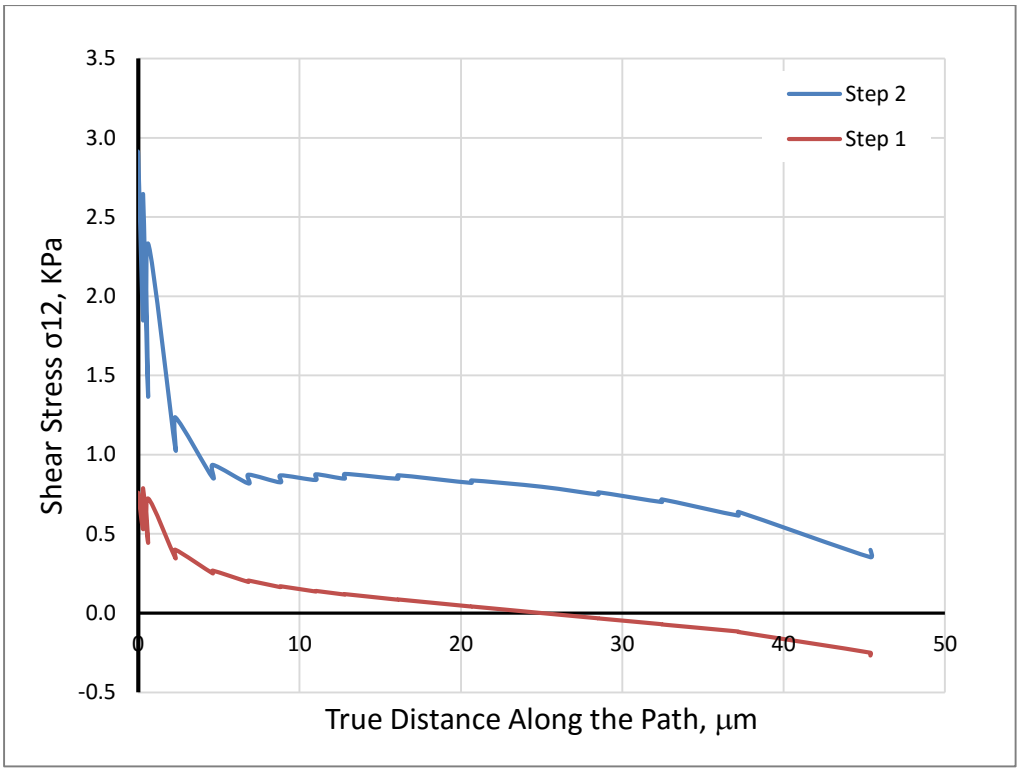

Figure 4.1. Shear stress σ12 for 2D PBM: cell contraction is obtained in step one, and shear load is applied on the top of cell surface in step two.

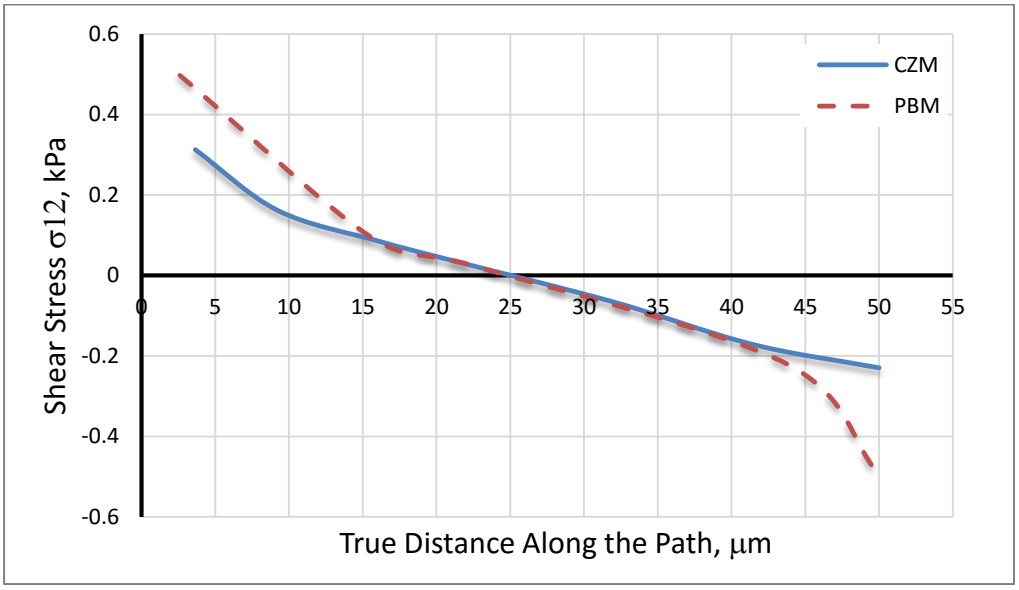

Figure 4.2. Shear stress σ12 for 2D CZM and 2D PBM at the interface of cell-substrate system: cell contraction is obtained in step one.

4.3. Investigation of the effects of fracture energy and contractile cell strain on the critical stress at separation

Six different cases are considered for cohesive zone model. These cases are listed in Table 4.1. Γc is interfacial fracture energy, which is the area under the traction-separation curve, (Fig 3.6). Ɛ is thermal strain due to cell contraction, ε_{therm}=Δα ΔT where T is temperature, Δα is the mismatch in thermal expansion coefficients in cell-substrate system. Thermal expansion coefficient for substrate is set to zero in all cases. Due to the limitation of ABAQUS cohesive element definition, only triangular shapes of traction separation properties are considered.

Table 4.1. Six different cases are investigated by cohesive model.

Case #	Interfacial Fracture Energy Γc, J/ m^2	Strain
1	1.0	0.00
2	1.0	0.05
3	1.0	0.10
4	0.1	0.00
5	0.1	0.05
6	0.1	0.10

Cohesive model describes crack nucleation and propagation at cohesive interface which is a function of displacement and separation. The cohesive bilinear model has three governing parameters: interface strength T_{max}, the characteristic length scale $\delta_{max}$and the decay length δ_c. σ_{max} and δ_{max} are varied to change the crack-bridging parameter. Interfacial fracture energy is calculated with the formula $\Gamma c = \frac{T_{max}\delta_c}{2}$, where T_{max} is interface strength, δ_c is characteristic length, the critical separation beyond which there is no traction. The ratio of T_{max}/δ_{max} controls reversible elastic stiffness, $K_c = T_{max}/\delta_{max}$. The viscosity coefficient is set to 0.001. The critical stress at separation of cell from substrate is calculated with formula:

$$\sigma_{critical} = \sigma * t,$$

where σ is shear load applied to the cell top surface, t is the step time calculated in ABAQUS when separation takes place at the interface.

The plot in Fig. 4.3 shows the calculated critical stress at separation of the interface as function of maximum traction force (interface strength) in 2D cohesive zone model. Six cases with different fracture energy and contractile cell strain are investigated in this study. The parameters used in the calculations are listed in Tables 4.2 – 4.7.

The effect of contractile cell strain on the critical stress at separation can be observed when toughness energy is constant. The highest critical stress at separation occurs when contractile cell strain is zero, and the lowest critical stress is observed when contractile cell strain is the highest (0.1). The critical stress at separation increases exponentially at lower $T_{max,}$ and there is a tendency to level it off to constant value at higher T_{max}.

Analysis of Fig. 4.5 shows the effect of toughness energy on the critical stress at separation when contractile cell strain is constant. The highest stress at separation corresponds to toughness energy equal to 1, and the lowest stress at separation corresponds to the lowest toughness energy (0.1). For example, if contractile cell strain ε =0.05, the critical stress at separation for Γc=1 is higher than for Γc=0.1. The same tendency is observed for the other two cases when contractile cell strain ε=0 and ε=0.1.

In addition, the effect of contractile cell strain can be compared to the effect of toughness energy to determine which of them produces greater effect on the critical stress at separation. The results of analysis indicate that the fracture energy effect on the critical stress is greater than the effect of contractile cell strain. If contractile cell strain varies and fracture energy is constant, the change in the critical stress of separation is not as large compared to the case when fracture energy varies and contractile cell strain is constant.

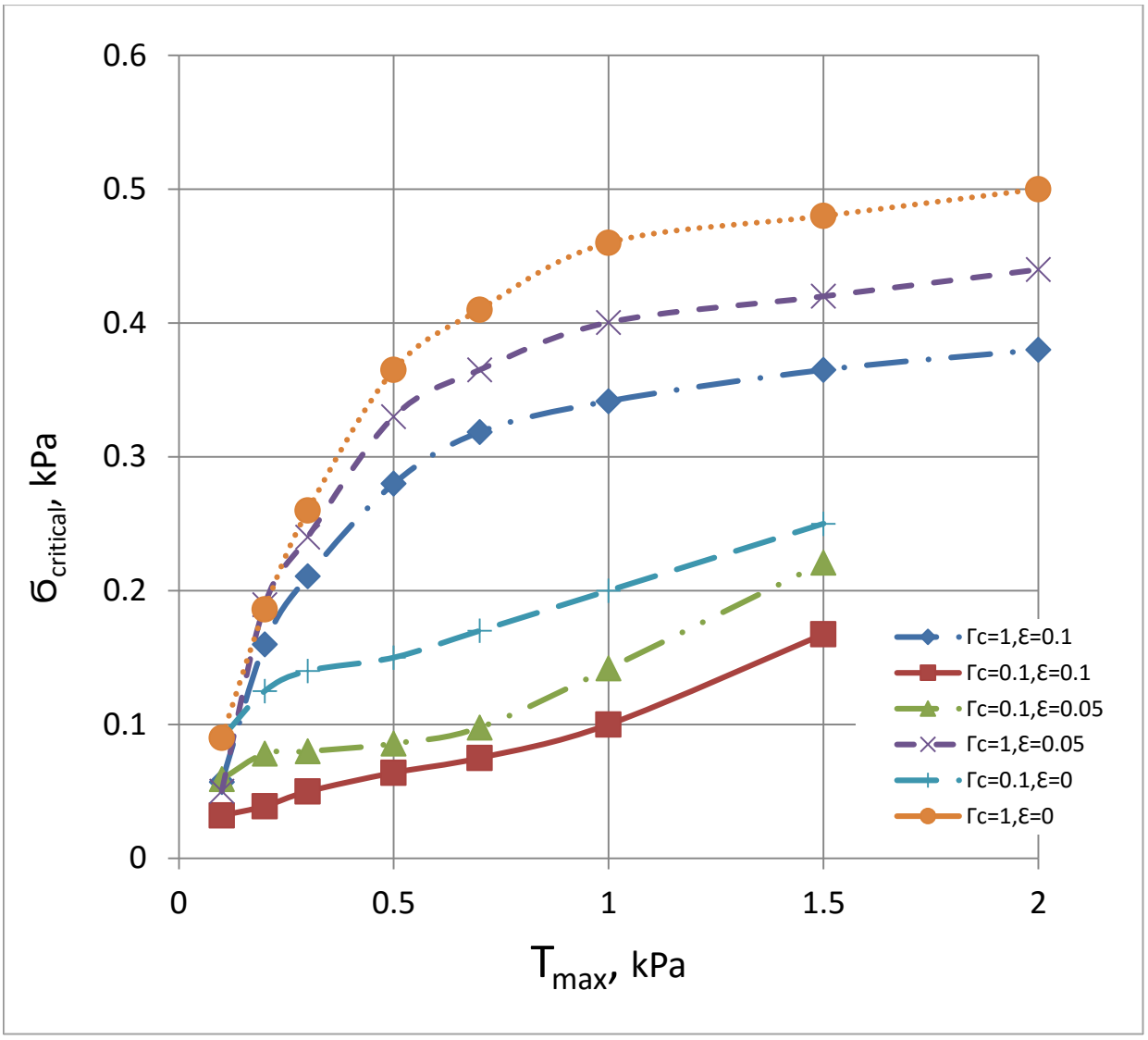

Figure 4.3. Critical stress at fracture of the interface as function of interface strength for 2D cohesive zone model for different cases listed in Table 4.1.

Table 4.2. Cohesive zone model for case 1 from Table 4.1 (Γc=1, Ɛ=0).

Kc, kPa/μm	**$T_{max,\ kPa}$**	**δ, μm**	**Load, kPa**	**Step Time, s**	**$б_{critical,\ kPa}$**
0.01	0.10	20.000	0.5	0.180	0.090
0.04	0.20	10.000	0.5	0.372	0.186
0.25	0.50	4.000	0.5	0.730	0.365
0.49	0.70	2.857	0.5	0.827	0.414
1.00	1.00	2.000	0.5	0.920	0.460
4.00	2.00	1.000	0.5	1.000	0.500

Table 4.3. Cohesive zone model for case 2 from Table 4.1 (Γc=1, Ɛ=0.05).

Kc, kPa/μm	**$T_{max,\ kPa}$**	**δ, μm**	**Load, kPa**	**Step Time, s**	**$б_{critical,\ kPa}$**
0.01	0.10	20.000	0.5	0.101	0.050
0.04	0.20	10.000	0.5	0.379	0.190
0.25	0.50	4.000	0.5	0.660	0.330
0.49	0.70	2.857	0.5	0.730	0.365
1.00	1.00	2.000	0.5	0.840	0.420
4.00	2.00	1.000	0.5	0.880	0.440

Table 4.4. Cohesive zone model for case 3 from Table 4.1 (Γc=1, Ɛ=0.1).

Kc, kPa/μm	**$T_{max,\ kPa}$**	**δ, μm**	**Load, kPa**	**Step Time, s**	**$б_{critical,\ kPa}$**
0.01	0.10	20.000	0.5	0.114	0.057
0.04	0.20	10.000	0.5	0.320	0.160
0.09	0.30	6.667	0.5	0.422	0.211
0.49	0.70	2.857	0.5	0.637	0.319
1.00	1.00	2.000	0.5	0.683	0.342
2.25	1.50	1.333	0.5	0.730	0.365
4.00	2.00	1.000	1.0	0.380	0.380

Table 4.5. Cohesive zone model for case 4 from Table 4.1 (Γc=0.1, Ɛ=0).

Kc, kPa/μm	**T_{max}, kPa**	**δ, μm**	**Load, kPa**	**Step Time, s**	**$б_{critical}$, kPa**
0.10	0.10	2.000	0.5	0.180	0.090
0.40	0.20	1.000	0.5	0.250	0.125
2.50	0.50	0.400	0.5	0.290	0.145
4.90	0.70	0.286	0.5	0.340	0.170
10.00	1.00	0.200	0.5	0.400	0.200
22.50	1.50	0.133	0.5	0.500	0.250
40.00	2.00	0.100	0.5	0.773	0.387

Table 4.6. Cohesive zone model for case 5 from Table 4.1 (Γc=0.1, Ɛ=0.05).

Kc, kPa/μm	**T_{max}, kPa**	**δ, μm**	**Load, kPa**	**Step Time, s**	**$б_{critical}$, kPa**
0.10	0.10	2.000	0.2	0.296	0.059
0.40	0.20	1.000	0.2	0.391	0.078
0.90	0.30	0.667	0.2	0.400	0.081
2.50	0.50	0.400	0.3	0.286	0.086
4.90	0.70	0.286	0.3	0.326	0.098
10.00	1.00	0.200	0.3	0.473	0.142
22.50	1.50	0.133	0.3	0.736	0.221
40.00	2.00	0.100	0.4	0.783	0.313

Table 4.7. Cohesive zone model for case 6 from Table 4.1 (Γc=0.1, Ɛ=0.1).

Kc, kPa/μm	**T_{max}, kPa**	**δ, μm**	**Load, kPa**	**Step Time, s**	**$б_{critical}$, kPa**
0.10	0.10	2.000	0.2	0.160	0.032
0.40	0.20	1.000	0.2	0.187	0.037
0.90	0.30	0.667	0.2	0.245	0.049
2.50	0.50	0.400	0.3	0.213	0.064
4.90	0.70	0.286	0.3	0.250	0.075
10.00	1.00	0.200	0.5	0.200	0.100
22.50	1.50	0.133	0.5	0.335	0.168
40.00	2.00	0.100	0.5	0.480	0.240

4.4. The role of the crack bridging characteristics in the transition from small-scale bridging (SSB) behavior to large-scale bridging (LSB) behavior

Bioadhesion is governed by the clustering of discrete bonds which can be considered as bridged crack. The role played by the crack bridging characteristics in the transition from SSB behavior to LSB behavior was investigated in [5], and it is confirmed in this study. The important parameter in this transition is the ratio $\frac{E\,\delta_{max}}{6_{max}}$ which defines the length scale and determines the size of the crack bridging zone. If $\frac{E\,\delta_{max}}{6_{max}} \ll a$ where a is crack size, it results in SSB behavior: the crack approaches the Griffith crack and exhibits fracture behavior of peeling a tape. LSB behavior happens if $\frac{E\,\delta_{max}}{6_{max}} \sim a$. This behavior leads to the uniform stress limit and exhibits behavior with the peanut butter effect at fracture. Clearly, de-adhesion process is controlled by the transition from SSB behavior to LSB behavior, and it is governed by the dimensionless parameter $\frac{E\,\delta_{max}}{6_{max}a}$. If $\frac{E\,\delta_{max}}{6_{max}a} \sim 1$then it follows LSB behavior. If $\frac{E\,\delta_{max}}{6_{max}a} \ll 1$ then it is Griffith crack with SSB behavior.

4.5. Shape effect on the critical stress at separation

3D CZM with irregular cell shape, (Fig. 4.4) and 3D CZM with circular cell shape are created to study shape effects on the critical stress at separation. The critical stress at separation is the highest for 2D CZM with circular cell shape, the lowest for 3D CZM with irregular cell shape, and in the middle range for 3D CZM with circular cell shape. The dependence of interface strength on the critical stress at separation follows exponential behavior when contractile strain varies and fracture energy equals to one. This dependence follows different law for the lowest fracture energy (0.1) (Fig. 4.5, a-d).

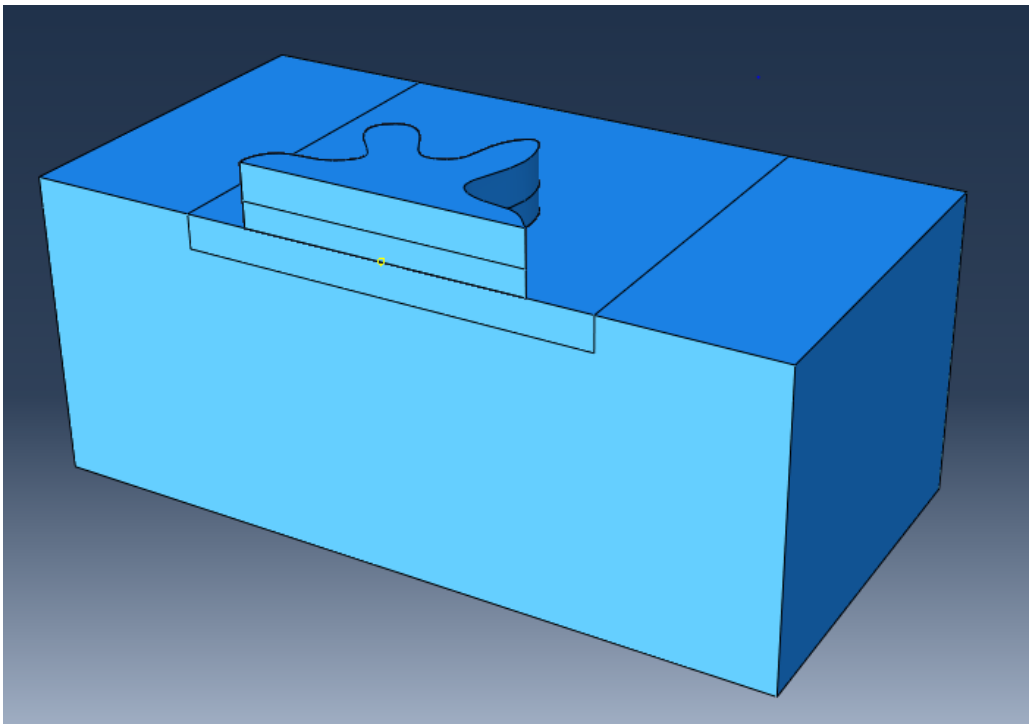

(a)

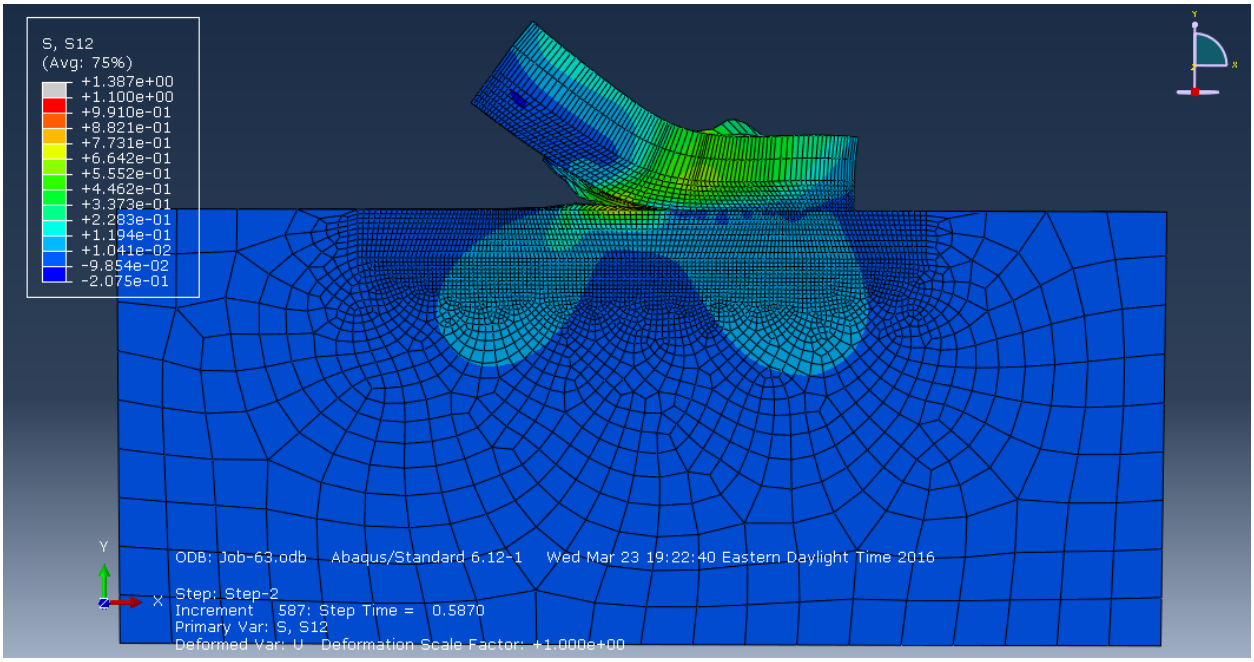

(b)

Figure 4.4. (a) 3D cohesive zone model with irregular cell shape; (b) Contour for shear stress Ϭ12 for 3D cohesive zone model with irregular cell shape for case three from Table 4.1.

Figure 4.5. The critical stress at separation as function of interface strength: (a) 2D CZM, 3D CZM with circular and irregular cell shape, for $\Gamma c=1$, $\mathcal{E}_{th}=0$; (b) 2D CZM, 3D CZM with circular and irregular cell shape, for $\Gamma c=1$, $\mathcal{E}_{th}=0.1$; (c) 2D CZM, 3D CZM with circular and irregular cell shape, for $\Gamma c=1$, $\mathcal{E}_{th}=0.05$; (d) 2D CZM, 3D CZM with circular and irregular cell shape for $\Gamma c=0.1$, $\mathcal{E}_{th}=0$.

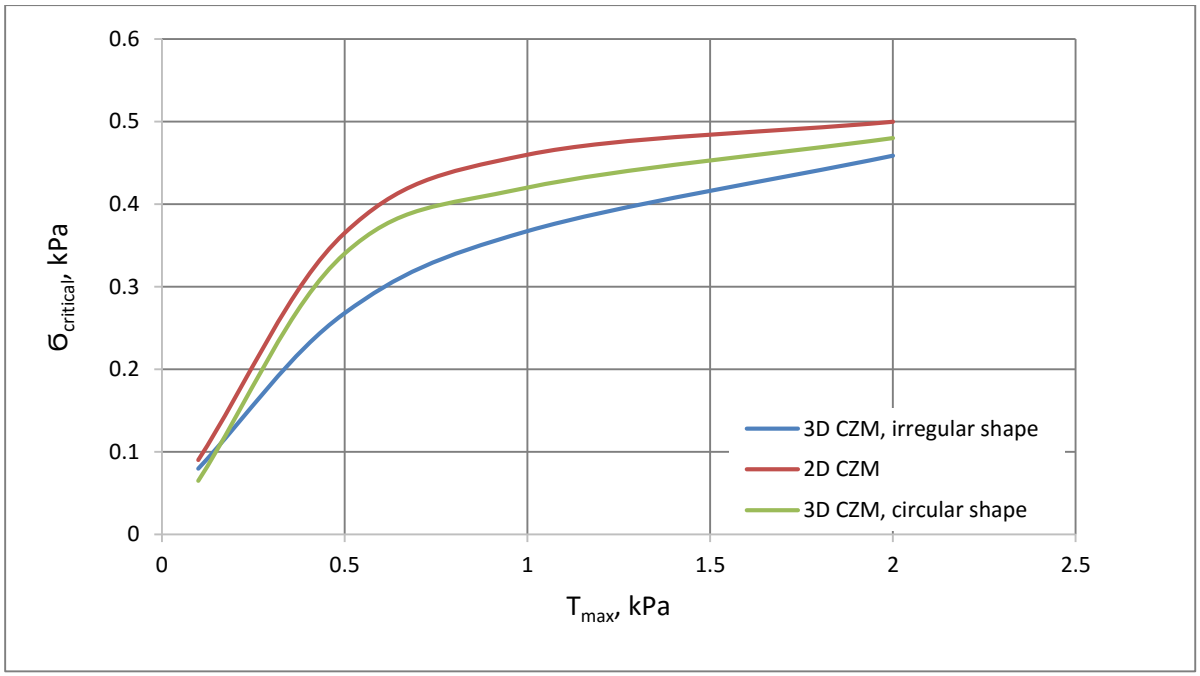

(a)

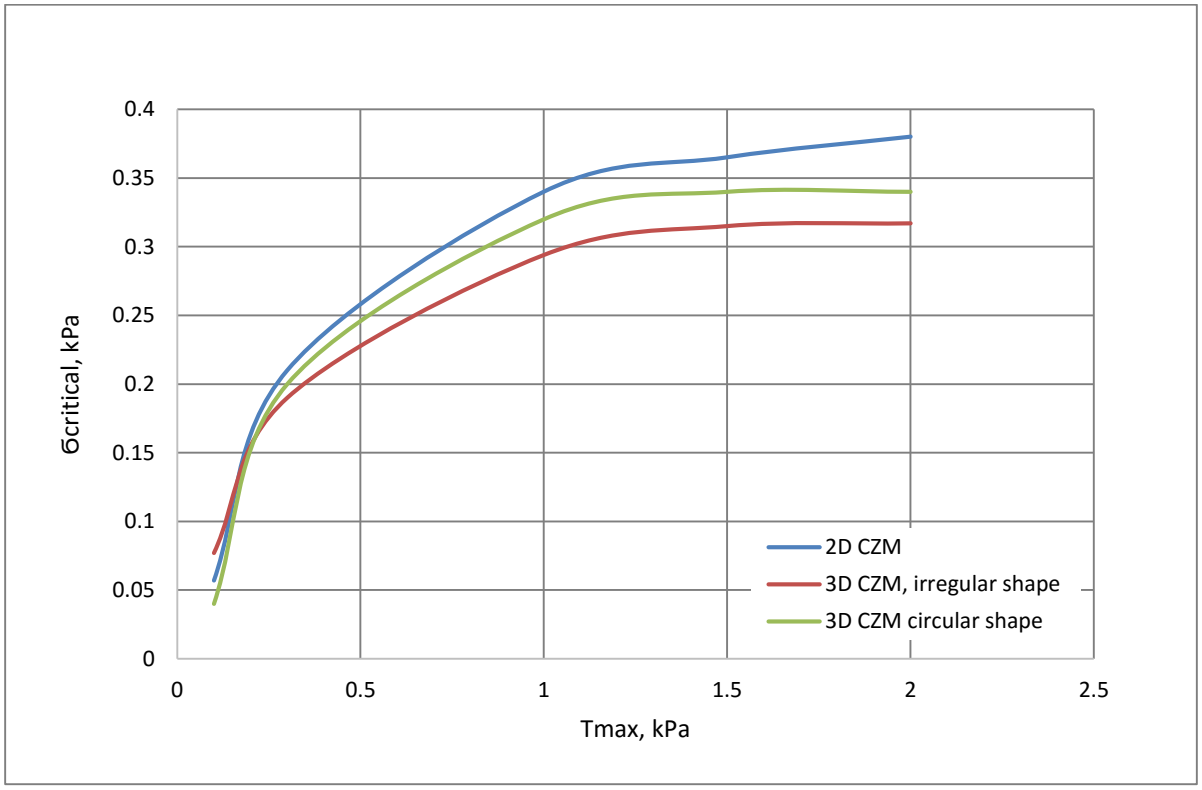

(b)

Figure 4.5. Continued

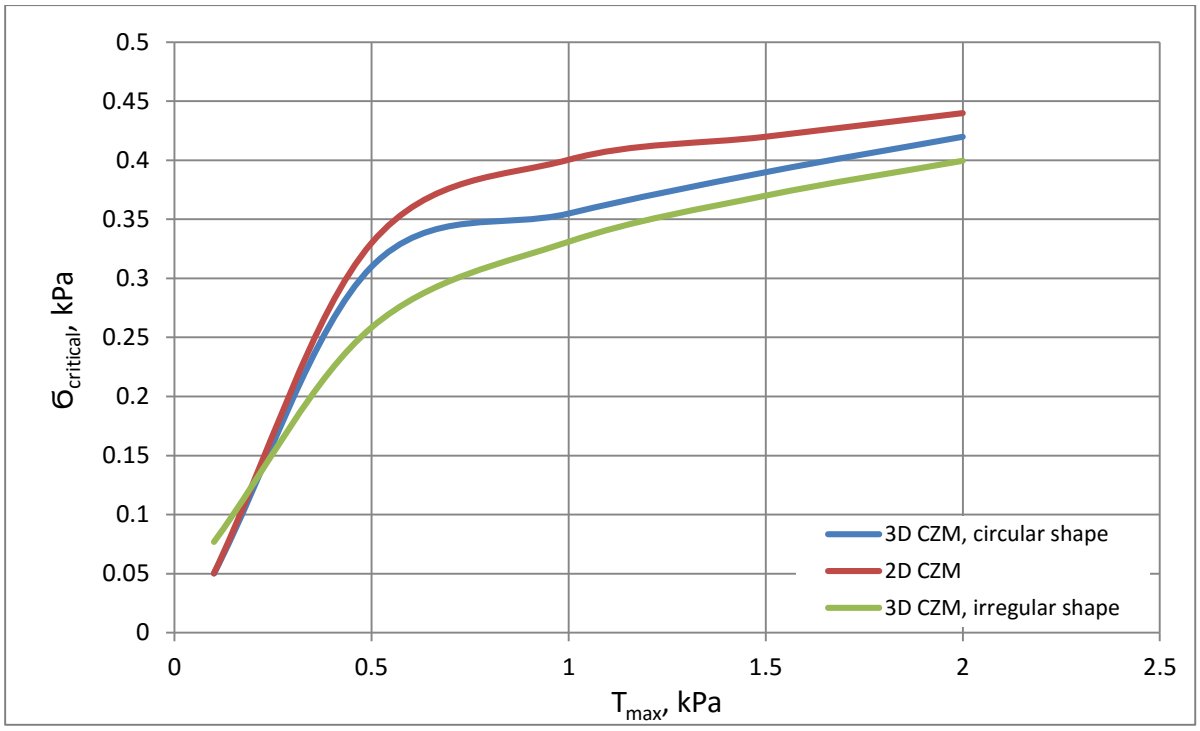

(c)

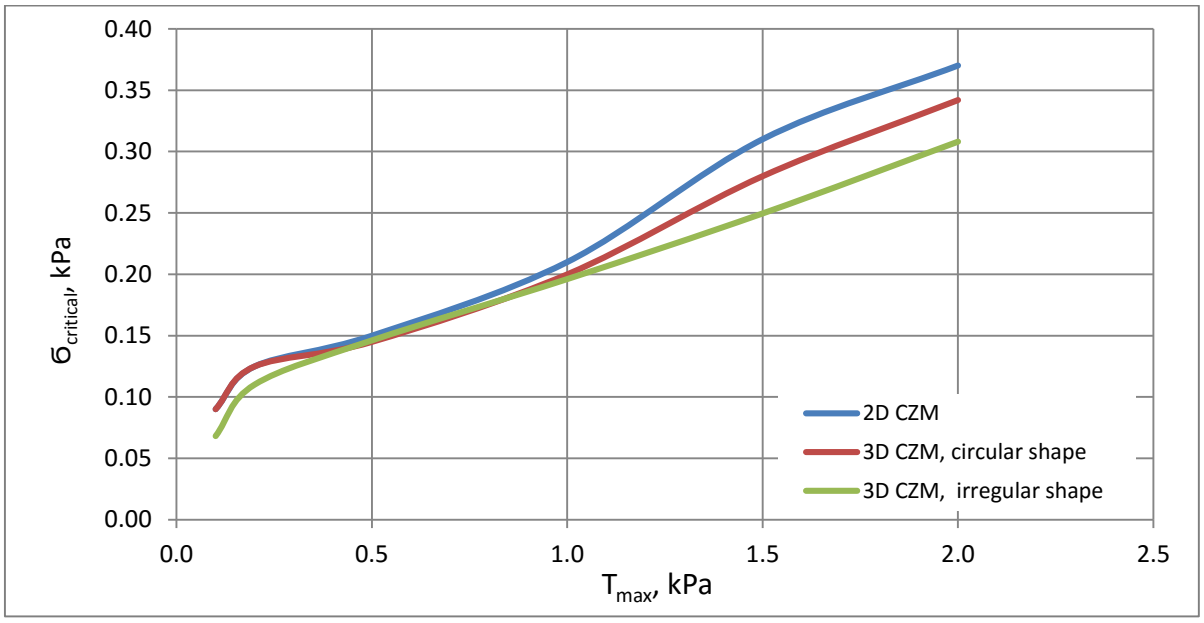

(d)

Figure 4.5. Continued

Chapter 5

Conclusions and Recommendations

The study of cell contraction, de-adhesion, and shape effects for potential applications aimed at an improved design of biomimetic and releasable adhesives has been conducted in this research. The research objectives are to study the effect of fracture energy on the critical stress at separation with constant contractile cell strain; the effect of contractile cell strain on the critical stress at separation with constant fracture energy and to compare both effects on the critical stress at separation. The additional objective is to study the effect of cell shape on the critical stress at separation and the role played by the crack-bridging characteristics in the transition from SSB behavior to LSB behavior. This research uses cohesive model with finite element simulations created with the commercial finite element software ABAQUS version 6.12. Cell is modeled as a pre-strained elastic disc which adheres on substrate with elastic isotropic material properties. Several models for cell-substrate system are created in this study: 2D perfect bonding model, 2D cohesive zone model and 3D cohesive zone model with circular and irregular cell shapes.

At the beginning of the study 2D perfect bonding model is created. There is no crack propagating at the interface in 2D perfect bonding model after the shear stress is applied as molecular bonds between cell and substrate are very strong. The stress field is calculated as the result of cell contraction achieved by the mismatch of thermal expansion coefficients in cell-substrate system and the reduction in temperature in step one. The shear load is applied to the cell top surface step two. It is shown that the shear stress 612 in step two is bigger that in step one.

Then the study is extended to 2D cohesive zone model, and the stress field is calculated. The contours of shear stress 612 for 2D cohesive zone model are obtained with cell contraction in the first step, and the shear load applied on the cell top surface in the second step. Plots of the shear stress applied on the cell top surface as function of true distance along the path at the interface are created and compared for 2D PBM and 2D CZM. In general, the magnitude of shear stress for perfect bonding model is greater than for cohesive zone model, although they overlap in the middle range of true distance along the path.

Since bioadhesive contacts are more complicated in real life, the study is extended to 3D cohesive zone model with circular and irregular cell shapes. Different cases are considered for 2D CZM and 3D CZM with circular and irregular cell shapes to investigate cell contraction, de-adhesion, and shape effects by cohesive model. Due to the limitation of ABAQUS cohesive element definition, only triangular shapes of traction separation properties are considered. The plots for the critical stress at separation of the interface as function of interface strength have been created with different fracture energy and contractile cell strain.

The effect of contractile cell strain on the critical stress at separation has been analyzed with constant fracture energy. The maximum value of the critical stress at separation occurs when contractile cell strain is zero, and the minimum critical stress occurs at the highest contractile strain. The critical stress at separation increases exponentially at lower interface strength, with the tendency to level it off to constant value at higher magnitude of interface strength.

In addition, the effect of fracture energy on the critical stress at separation with constant contractile cell strain has been studied. The results of the study indicate that the critical stress at separation increases with fracture energy. The highest stress at separation corresponds to fracture

energy equal to 1, and the lowest stress at separation corresponds to the lowest fracture energy (0.1).

The effects of contractile cell strain and fracture energy on the critical stress at separation are compared, and the latter produces greater effect than the former. If contractile cell strain varies at constant fracture energy, the change in the critical stress at separation is not as large compared to the case when fracture energy varies at constant contractile cell strain.

The role played by the crack bridging characteristics in the transition from SSB behavior to LSB behavior investigated in [5] is confirmed in this study. This transition is governed by the ratio of the crack bridging zone size to the contact radius. This parameter has a very important consideration in the design of technological products aimed at the optimization of adhesion force. Also, shape effect on the critical stress at separation has been investigated, and it is shown that the critical stress at separation is the highest for 2D CZM, the lowest for 3D CZM with irregular cell shape, and in the middle range for 3D CZM with circular cell shape.

The obtained results can shed light on the design of biomimetics and releasable adhesives. One of the potential applications aimed at the improvement of bio-adhesive properties is that the critical shear stress at separation can be optimized by tuning material stiffness and interface strength. Also, the initial contact shape can be arranged to maximize adhesion force in bio-adhesive contacts by manipulating the transition from SSB behavior to LSB behavior.

A number of open questions can be further explored in future work. It will be interesting to study cell contraction and interface fracture process of long - chain molecules in bioadhesive contacts for anisotropic and spatially constrained substrate. During fracture of long-chained molecules it is assumed that bond density is the same across the entire interface. However, in real

life bond density varies, so that it can be explored further by assigning different constitutive parameters along the interface in bioadhesive contacts.

List of References

[1] He, S., Su, Y., Ji, B., & Gao, H., 2014, "Some basic questions on mechano-sensing in cell-substrate interaction," *Journal of the Mechanics and Physics of Solids*, 70, 116-135.

[2] Yang, X. & Robinson, J.R., 1998, "Bioadhesion in mucosal drug delivery". In: Okano T., Editor, *Biorelated Polymers and Gels: Controlled Release and Applications in Biomedical Engineering*. Academic Press, Boston, MA, 135-192.

[3] Dembo, M. & Wang, Y.L., 1999, "Stresses at the cell-to-substrate interface during locomotion of fibroblasts," *Biophysical Journal*, 76 (4), 2307-2316.

[4] Munevar, S., Wang, Y.L., & Dembo, M., 2001, "Distinct roles of frontal and rear cell-substrate adhesions in fibroblast migration," *Molecular Biology of the Cell*, 12 (12), 3947-3954.

[5] Liu, Y. & Gao, Y., 2015, "Non-uniform breaking of molecular bonds, peripheral morphology and releasable adhesion by elastic anisotropy in bio-adhesive contacts," *Journal of the Royal Society Interface*, 102 (12), 214-242.

[6] Wang, J. & Gao, H, 2010, "Size and shape dependent steady state pull-off force in molecular adhesion between soft elastic materials," *International Journal of Fracture*, 166 (1-2), 13-19.

[7] Liu, Y., Liu, H., & Gao, Y., 2015, "Can mushroom-shaped fibers enhance the bio-adhesive performance?" *Journal of Mechanics in Medicine and Biology*, 15 (5), Article no. 1550068.

[8] Gao, H., Ji, B., Jager, I.L., Arz, E., & Fratzl, P., 2003, "Materials become insensitive to flaws at nanoscale: lessons from nature," *Proceedings of the National Academy of Sciences of the United States of America*, 100 (10), 5597-5600.

[9] Rape, A.D., Guo, W.H., & Wang, Y.L., 2011, "The regulation of traction force in relation to cell shape and focal adhesions," *Biomaterials*, 32 (8), 2043-2051.

[10] Gardel, M.L., Sabass, B., Ji, L., Danuser, G., Scwartz, U. S., & Waterman, C.M., 2008, "Traction stress in focal adhesions correlates biphasically with actin retrograde flow speed," *Journal of Cell Biology*, 183 (6), 999-1005.

[11] Wang, N., Ostuni, E., Whitesides, G.M., & Ingber, D.E., 2002, "Micropatterning tractional forces in living cells," *Cell Motility and the Cytoskeleton*, 52 (2), 97-106.

[12] Chen, S. & Gao, H., 2006, "Non-slipping adhesive contact between mismatched elastic spheres: A model of adhesion mediated deformation sensor," *Journal of the Mechanics and Physics of Solids*, 54 (8), 1548-1567.

[13] Lemmon, C.A. & Romer, L.H., 2010, "A predictive model of cell traction forces based on cell geometry," *Biophysical Journal*, 99 (9), L78-L80.

[14] Edwards, C.M. & Scwartz, U.S., 2011, "Force localization in contracting cell layers," *Physical Review Letters*, 107 (12), Publication no. 128101.

[15] Engler, A.J., Sen, S., Sweeney, H.L., & Discher, D.E., 2006, "Matrix elasticity directs stem cell lineage specification," *Cell*, 126 (4), 677-689.

[16] Sen, S., Engler, A.J., & Discher, D.E., 2009, "Matrix strains induced by cells: Computing how far cells can feel," *Cellular and Molecular Bioengineering*, 2 (1), 39-48.

[17] Deshpande, V.S., Mrksich, M., McMeeking, R.M., & Evans, A.G., 2008, "A bio-mechanical model for coupling cell contractility with focal adhesion formation," *Journal of the Mechanics and Physics of Solids*, 56 (4), 1484-1510.

[18] Chang, S.S., Guo, W.H., Kim, Y., & Wang, Y.L., 2013, "Guidance on cell migration by substrate dimension," *Biophysical Journal*, 104 (2), 313-321.

[19] Fu, J., Wang, Y.K., Yang, M.T., Desai, R.A., Yu, X., Liu, Z., & Chen, S.C., 2010, "Mechanical regulation of cell function with geometrically modulated elastomeric substrates," *Nature Methods*, 7 (9), 733-736.

[20] Ladoux, B., Anon, E., Lambert, M., Rabotzey, A., Hersen, P., Buguin, A., Silberzan, P., & Mege, R.M., 2010, "Strength dependence of cadherin-mediated adhesions," *Biophysical Journal*, 98 (4), 534-542.

[21] Deguchi, S., Ohashi, T., & Sato, M., 2006, "Tensile properties of single stress fibers isolated from cultured vascular smooth muscle cells," *Journal of Biomechanics*, 39 (14), 2603-2610.

[22] Bower, A., 2009, *Applied mechanics of solids*. CRC Press, Taylor & Francis Group, Boca Raton, FL.

[23] Bao, G. & Suo Z., 1992, "Remarks on crack-bridging concepts," *Applied Mechanics Reviews*, 45 (8), 355-366.

[24] Gao, Y.F. & Bower, A.F., 2004, "A simple technique for avoiding convergence problems in finite element simulations of crack nucleation and growth on cohesive interface," *Modelling and Simulation in Materials Science and Engineering*, 12, 453-463.

[25] Gao, Y.F. & Bower, A.F., 2006, "Elastic-plastic contact of a rough surface with Weierstrass profile," *Proceedings of Royal Society London, Series A*, 462, 319-348.

[26] Yao, H. & Gao H., 2006, "Mechanics of robust and releasable adhesion in biology: bottom-up designed hierarchical structure of gecko," *Journal of the Mechanics and Physics of Solids*, 54 (6), 1120–1146.

[27] Liu, Y. & Gao Y., 2016, "Nonuniform breaking of molecular bonds, peripheral morphology, and releasable adhesion by elastic anisotropy in bio-adhesive contacts," *Bio Nano Interfaces and Engineering Applications Symposium, 2016 TMS Annual Meeting*, Nashville, TN, February 18, 2016.

Vita

Margarita Petrova was born in Moscow, Russia. She graduated with the diploma of training engineering on machine building with Master's degree from Moscow State Technical University "MAMI" (Moscow, Russia). From 1998 to 2003 she worked as staff instructor in the Engineering Graphics Department at Moscow Power Institute (Technical University) "MPI" (Moscow, Russia). At the same period of time she also collaborated with the Scientific Research Center for Wear Resistance on projects aimed at the increase in reliability of thermal equipment and the protection of power plant components against corrosive environment. After moving to the United States, she worked from 2007 to 2014 as adjunct instructor in Engineering and Media Technologies Department at Pellissippi State Community College (Knoxville, TN) and as tax accountant. She enrolled in the graduate school at the University of Tennessee (Knoxville, TN) and worked as graduate research assistant under the guidance of Dr. Gao Y. and Dr. He W. in the Department of Material Science and Engineering. She completed her Master's degree in May 2016.